PERGAMON

International Journal of Heat and Mass Transfer 43 (2000) 473–485

International Journal of HEAT and MASS TRANSFER

www.elsevier.com/locate/ijhmt

The effects of duct inclination angle on laminar mixed convective flows over a backward-facing step

Hiroshi Iwai[a,*], Kazuyoshi Nakabe[a], Kenjiro Suzuki[a], Koji Matsubara[b]

[a]*Department of Mechanical Engineering, Kyoto University, Kyoto 606-8501, Japan*
[b]*Graduate School of Science and Technology, Niigata University, Niigata 950-2102, Japan*

Received 18 September 1998; received in revised form 11 March 1999

Abstract

Three-dimensional numerical simulations were carried out for mixed convective flows over a backward-facing step in a rectangular duct. Reynolds number, expansion ratio and aspect ratio were kept constant at $Re = 125$, $ER = 2$ and $AR = 16$, respectively. Heat flux at the wall downstream of the step was kept uniform, while other walls were kept at adiabatic condition. Effect of the inclination angles, θ_1, θ_2, was the main objective in this study. It was found that when θ_1 was varied, the effect of buoyancy became prominent at $\theta_1 = 0^\circ$, 180°, while the effect was relatively small for the two horizontal cases ($\theta_1 = 90^\circ$, 270°). However, there was still small difference between $\theta_1 = 90^\circ$ and 270° in the region immediately after the step where the flow was relatively slow. When θ_2 was varied, flow and thermal fields became asymmetric about the duct centerline, except when $\theta_2 = 0^\circ$, 180°. The maximum Nusselt number, which appears symmetrically near the side walls in pure forced convection cases, was obtained at only one location close to the lower side wall.

Keywords: Numerical simulation; Backward-facing step; Low Reynolds number; Mixed convection; Inclination angle

1. Introduction

The flows inside the recent compact heat exchangers can be laminar. In such heat exchangers, flow separation and reattachment phenomena are often used to modify the flow field, for establishing a favorable heat exchange. Therefore it is very important to understand the details of the flow separation and reattachment phenomena for laminar flows. As the most typical problem, flows over a backward-facing step have attracted considerable attention. The authors have previously investigated the influence of the duct aspect ratio on the flow and thermal fields at low Reynolds numbers for the flows in a rectangular duct with a sudden expansion [1]. Although the buoyancy effects were not taken into consideration in the previous study, it should become significant if the temperature difference between fluid and the wall is relatively large [2–4]. Considering that a low Reynolds number flow is sensitive to the buoyancy effects, it is important to study how its effect is.

Recently, Baek et al. [5] and Abu-Mulaweh et al. [6,7] measured experimentally the velocity and temperature distributions in buoyancy affected backward-facing step flows. Lin et al. [8,9] and Hong et al. [10] performed two-dimensional simulations for similar flows, varying the buoyancy level, inclination angle of the duct and Prandtl number. However, there are many parameters in this system and the details of

* Corresponding author. Tel.: +81-75-753-5218; fax: +81-75-771-7286.
E-mail address: iwai@htrans.mech.kyoto-u.ac.jp (H. Iwai)

0017-9310/00/$ - see front matter
PII: S0017-9310(99)00141-6

Nomenclature

AR	aspect ratio, WD/S
C_f	skin friction coefficient, $2\tau_w/\rho U_{in}^2$
C_P	specific heat
ER	expansion ratio, $H/(H-S)$
g	acceleration of gravity
Gr^*	modified Grashof number, $\rho^2 g\beta q_w S^4/\mu^2\lambda$
H	duct height
h	enthalpy
Nu	Nusselt number, $q_w S/\lambda(T_w - T_{in})$
P	pressure
q	heat flux
Re	Reynolds number, $\rho U_{in} S/\mu$
Ri^*	modified Richardson number, Gr^*/Re^2
S	step height
T	temperature
T_{in}	inlet temperature
t	time
U	velocity component in x-direction
U_{in}	cross-sectional mean velocity at the inlet
V	velocity component in y-direction
W	velocity component in z-direction
WD	duct width
x	streamwise coordinate
y	transverse coordinate
z	spanwise coordinate
β	cubic expansion coefficient
θ_1	pitch angle of the duct
θ_2	rolling angle of the duct
λ	thermal conductivity
μ	fluid viscosity
ρ	density
τ	shear stress, $\mu\frac{\partial U}{\partial y}$

Subscripts

max	maximum Nusselt number and its position or maximum value in a cross section
min	minimum value in a cross section
p	peak Nusselt number point
r	reattachment point
s	secondary recirculation region
w	wall surface

flows are not clear yet. Especially, to the author's knowledge, no three-dimensional study on the effects of inclination angles has been previously reported in the literature.

In this study, 3D simulations are carried out for mixed convective flows over a backward-facing step in a duct. Attention is paid to the effects of the two inclination angles of the flow configuration: one is the pitch angle and the other is the rolling angle to be defined later.

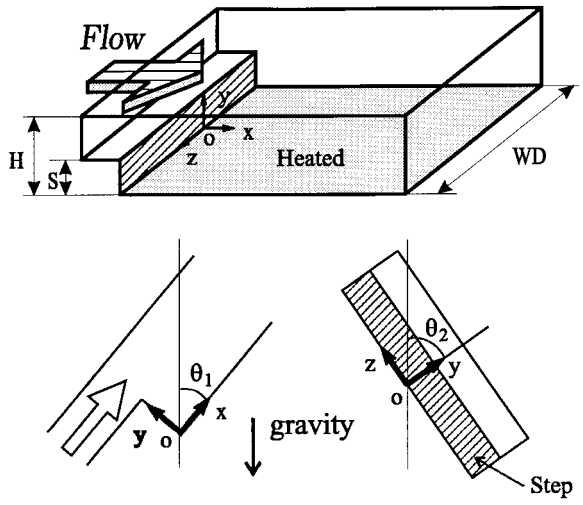

Fig. 1. Computational domain.

2. Computational method

The computational domain is schematically illustrated in Fig. 1. The computational domain covers $-1 \le x/S \le 30$, where S is the step height. It was confirmed that adoption of a longer streamwise size of computational domain did not change the final results. Unsteady Navier–Stokes and energy equations are solved numerically together with the continuity equation using the finite difference method.

$$\frac{\partial \rho}{\partial t} + \nabla \cdot \left(\rho \vec{U}\right) = 0 \tag{1}$$

$$\frac{\partial}{\partial t}\left(\rho \vec{U}\right) + \nabla\left(\rho \vec{U}\vec{U}\right) = -\nabla P + \mu \nabla^2 \vec{U} + \frac{\rho\beta}{C_P}(h - h_0)\vec{g} \tag{2}$$

$$\frac{\partial}{\partial t}(\rho h) + \nabla \cdot \left(\rho \vec{U} h\right) = \nabla \cdot \left(\frac{\lambda}{C_P}\nabla h\right) \tag{3}$$

here after U, V, W will be used instead of $\vec{U}$. They stand for velocity components for x-, y- and z-direction, respectively. A fifth-order upwind scheme and a

fourth-order central difference scheme are adopted for the convection and diffusion terms of the governing equations, respectively. Properties of the working fluid (air) are assumed to be constant, and the Boussinesq approximation [3] is used to evaluate the buoyancy term. Prandtl number is set at 0.71. SIMPLE algorithm [11] is used for the computation of pressure correction in the iteration procedure.

At the upstream boundary, inlet flow is assumed to be hydrodynamically steady and fully developed and to have a uniform temperature profile. U profile is assumed to obey the approximation proposed by Shah and London [12], while V and W are set to be zero. No-slip condition is applied at the all wall surfaces. The heated wall downstream of the step is maintained at a uniform heat flux, while the top and bottom straight walls, the backward-facing wall and the side walls are assumed to be thermally adiabatic. Streamwise gradients of all quantities at the duct exit are set to be zero.

A maximum of $140 \times 36 \times 87$ grid points are allocated non-uniformly in the computational domain, finely in the near-wall regions where large gradients of velocity and temperature are expected. The smallest grid spacing, $\Delta x_{\min}$ in the above mentioned finest grid system is $0.05S$. The time increment between two successive time steps is set so that the Courant number for the smallest grid spacing is equal to unity.

Reynolds number, the expansion ratio and the aspect ratio are kept constant at $Re = 125$, $ER = 2$ and $AR = 16$, respectively. It was confirmed that both the flow and thermal fields can be considered as 2D around the center region of the heated wall under such conditions, if buoyancy is neglected.

The main interest in this study is the effects of two inclination angles, θ_1 and θ_2 described in Fig. 1, over the flow and thermal fields. They are defined as below:

- θ_1, pitch angle: an angle between the streamwise direction and vertical upward direction and its changing range is $0^\circ \le \theta_1 \le 360^\circ$.
- θ_2, rolling angle: an angle between the normal direction and vertical upward direction, $0^\circ \le \theta_2 \le 180^\circ$.

The duct posture is determined by specifying these inclination angles.

Calculations are carried out in the first stage of this study for several cases of different modified Richardson number, Ri^*, for the two extreme cases, upward and downward flows, in order to select the buoyancy level at which the effects of inclination angles should be investigated. Ri^* is varied at this first stage in the range of $0 \le Ri^* \le 0.12$. Variation of Ri^* is equivalent to varying the heat flux for a given step height. The computational conditions are chosen so that the maximum temperature difference between the main flow and the heated wall becomes approximately

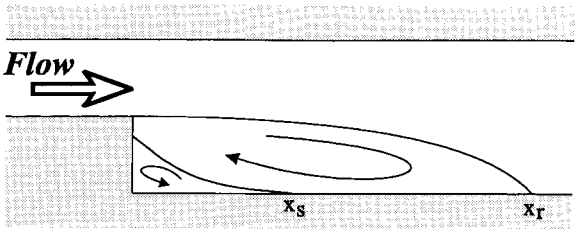

Fig. 2. Main and secondary recirculation regions.

20 K for the case of 10 mm step height, which should be a normal size to be adopted in experiments. The effects of inclination angles, θ_1 and θ_2, are studied, keeping Ri^* at a constant value to be chosen as the results of the first stage computation. θ_1 is first changed in the range of $0^\circ \le \theta_1 \le 360^\circ$ with θ_2 kept at 0°. The case of $\theta_1 = 0^\circ (= 360^\circ)$ is equivalent to the upward flow case while $\theta_1 = 180^\circ$ to the downward flow. Finally θ_2 will be changed in the range of $0^\circ \le \theta_2 \le 180^\circ$ keeping θ_1 constant at 90° and its effects will be studied. The case of $(\theta_1, \theta_2) = (270^\circ, 0^\circ)$ and $(90^\circ, 180^\circ)$ are the same posture to each other.

The local velocity and temperature at several grid points are monitored at each time step and if the fluctuations of those values decrease to less than a certain criteria (e.g. 0.1% of U_{in} for the transverse velocity, V), the flow and thermal fields are considered steady. The flows were found to remain steady in all the cases calculated. All calculations were performed on the VP2600 computer at the Kyoto University Data Processing Center. One iteration required approxi-

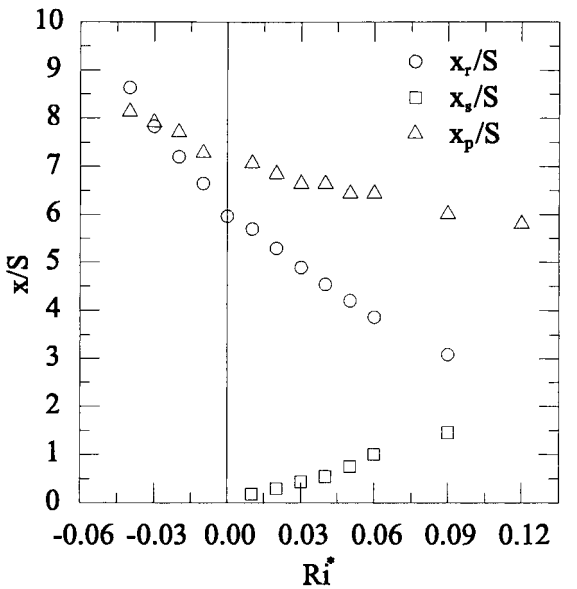

Fig. 3. Effect of Ri^* on x_r, x_p and x_s.

mately 0.6 s when the total number grid points was about 4×10^5.

3. Results and discussion

3.1. Ri^* effects on up/downward flows

The effects of Ri^* on the three positions of the reattachment point x_r, the peak Nusselt number point x_p and the downstream end of the secondary recirculation region x_s are discussed here. The peak Nusselt number here means the maximum Nusselt number along the centerline of the heated wall. The secondary recirculation region is defined as the recirculation region which appears at the corner of the step, inside of the main recirculation zone with an opposite direction of recirculating flow and is schematically illustrated in Fig. 2. The value of x_s is defined as the distance from the step to a position where the sign of skin friction coefficient changes from positive to negative. The positions of x_r, x_p and x_s obtained along the centerline of the heated wall are presented in Fig. 3 for both upward ($Ri^* > 0$) and downward ($Ri^* < 0$) flows. Although the value of Ri^* should be always positive in nature, negative value is assigned for convenience in Fig. 3 for downward flows heated from the wall.

The buoyancy level, or the value of Ri^*, clearly affects the positions plotted in Fig. 3. As the absolute value of Ri^* is increased, the reattachment position, x_r, and the peak Nusselt number position, x_p, move upstream in the upward flow case ($Ri^* > 0$) and move downstream in the downward flow case ($Ri^* < 0$). x_r is located downstream of x_p when $Ri^* = -0.04$. When $Ri^* = -0.03$, they are closely located to each other. For $Ri^* \geq -0.02$, x_r always appears upstream of x_p. The distance between x_r and x_p becomes longer as Ri^* increases. The secondary recirculation region exists only in the upward flow cases ($Ri^* > 0$). x_s moves downstream as Ri^* increases. x_r and x_s are expected to merge in when Ri^* is increased above 0.09. In that case the main recirculation region detaches from the heated wall [8].

Abu-Mulaweh et al. [7] reported that x_r increased considerably with a small increase of Ri^* in the downward flow case ($Ri^* < 0$), or in the present manner of description, with a small decrease of Ri^* from zero. The same tendency is observed in the present simulation. The value of x_r increases with decrease of Ri^* in downward flow cases, resulting in a stronger and longer main recirculation region downstream of the step. This results from the reinforcement of the reverse flow inside the main recirculation region produced by the buoyancy acting on the relatively high temperature fluid existing near the heated wall. At $Ri^* = -0.05$, the calculation was no longer stable. Considering the above results, the effects of θ_1 and θ_2 will be studied in the following by keeping Ri^* equal to 0.03.

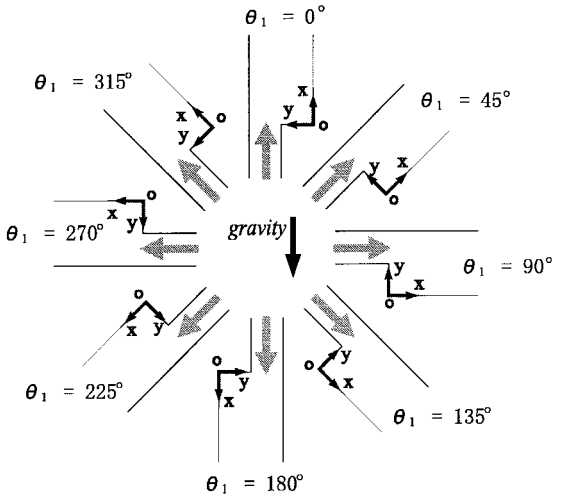

Fig. 4. Change of duct posture with θ_1.

3.2. Effects of the pitch angle θ_1

The effects of θ_1 is examined first. θ_1 is changed from 0° to 360° while θ_2 is kept constant at 0°. This is schematically illustrated in Fig. 4. $\theta_1 = 0°$ and 180° correspond to the upward and downward flows, respectively. The flow is accelerated in the x-direction by the buoyancy at the pitch angle in the ranges $0° \leq \theta_1 < 90°$ and $270° < \theta_1 \leq 360°$. Hong et al. [10] studied a similar case by conducting a 2D simulation.

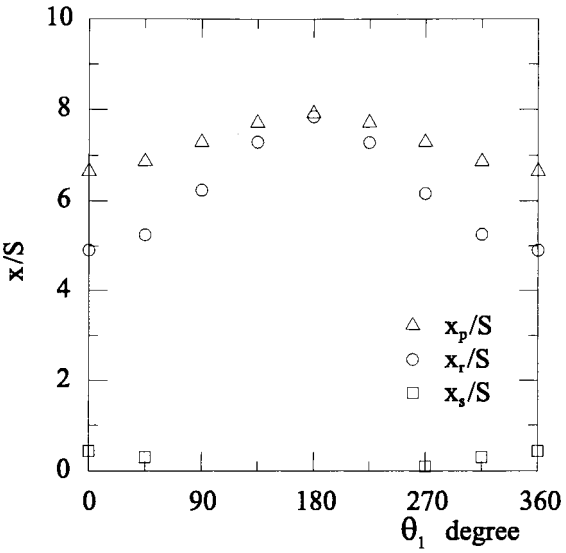

Fig. 5. Effect of θ_1 on x_r, x_p and x_s (3D).

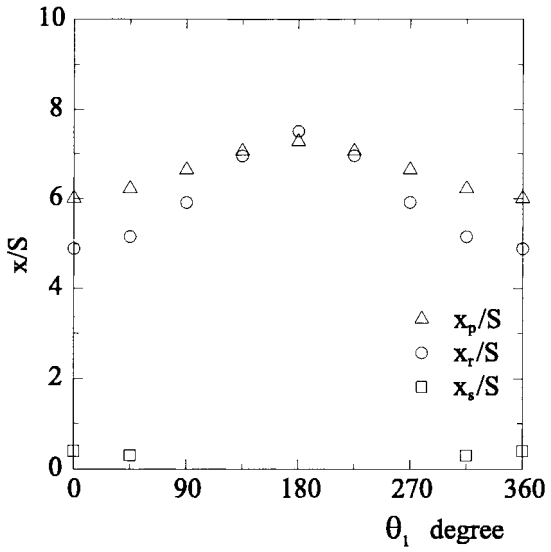

Fig. 6. Effect of θ_1 on x_r, x_p and x_s (2D).

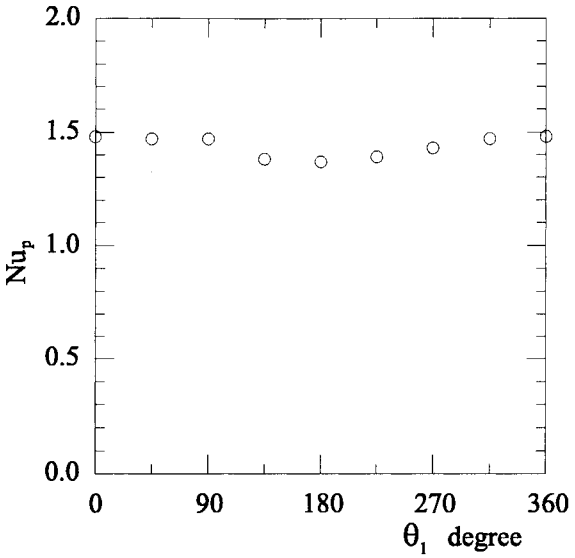

Fig. 7. Effect of θ_1 on the peak Nu along the centerline (3D).

They did a computation for the condition of $Re = 100$ and $Gr^* = 609$, where the buoyancy level, Ri^*, is expected to be twice as large as that of the present study.

The effects of θ_1 on the positions of the reattachment point, x_r, the peak Nusselt number point, x_p, and the secondary recirculation region, x_s, along the centerline of the heated wall are shown in Fig. 5. The results qualitatively match the results obtained by Hong et al. [10]. As θ_1 increases, the value of x_r and x_p increase when $0^\circ \le \theta_1 \le 180^\circ$ and decrease when $180^\circ \le \theta_1 \le 360^\circ$. Hong et al. [10] reported that the relative positions of x_r and x_p switched at a certain pitch angle and that in the range of $120^\circ < \theta_1 < 240^\circ$ x_r was located downstream of x_p. This phenomenon is not observed in the present 3D simulations. The peak Nusselt number point x_p always appears at a position further downstream of the reattachment point x_r in Fig. 5. The distance between the two points is found to reach a maximum value at $\theta_1 = 0^\circ (360^\circ)$ and a minimum value at $\theta_1 = 180^\circ$. Hong et al. [10] also reported that the changing pattern of the three positions with a change of θ_1 was asymmetric about $\theta_1 = 180^\circ$. However, this asymmetry is smaller in Fig. 5 compared to Hong's results [10]. Fig. 5 shows that the end position of the secondary recirculation region, x_s, marks its maximum value at $\theta_1 = 0^\circ$. No secondary recirculation is observed in the range of the pitch angle $90^\circ \le \theta_1 \le 225^\circ$.

2D simulations under the same computational conditions as the ones shown in Fig. 5 are performed to be compared with the results of 3D simulations. The results of 2D simulations are shown in Fig. 6. The switching phenomenon of the positions of x_r and x_p is observed at $\theta_1 = 180^\circ$ in Fig. 6. It implies that 2D assumption can affect the relative position of x_r and x_p. The relative spatial positions of these two points should be discussed carefully. The asymmetry of the changing patterns of x_r, x_p and x_s positions about $\theta_1 = 180^\circ$ in the 2D simulations shown in Fig. 6 is even smaller than that of present 3D simulations shown in Fig. 5. This suggests that the stronger asymmetry reported by Hong et al. [10] is not due to the 2D assumption but probably related to the larger buoyancy level employed in his study.

Fig. 7 shows the effect of θ_1 on the value of peak Nusselt number, Nu_p, for the results of 3D simulations. Peak Nusselt number marks its maximum at $\theta_1 = 0^\circ$ and minimum at $\theta_1 = 180^\circ$. The difference between the maximum and minimum is approximately 7% of the average value of Nu_p.

The contours of the skin friction coefficient C_f on the heated wall are shown in Fig. 8 for four different values of θ_1 (0°, 90°, 180°, 270°). The shaded area corresponds to the area where the skin friction coefficient is positive in sign. The borderlines between the shaded area and the white area correspond to the positions of x_s and x_r. In all the cases, a 2D region can be observed in the middle of the heated wall, where the contourlines are almost parallel to the z-axis. The 2D region seems to be narrower in the case of $\theta_1 = 180^\circ$ compared to other three cases. It is obviously seen in Fig. 8 that the cases of $\theta_1 = 90^\circ$ and 270° have C_f distribution patterns on the entire heated wall quite similar to each other. This suggests that buoyancy effect is not large for horizontal flow at the buoyancy level of $Ri^* = 0.03$.

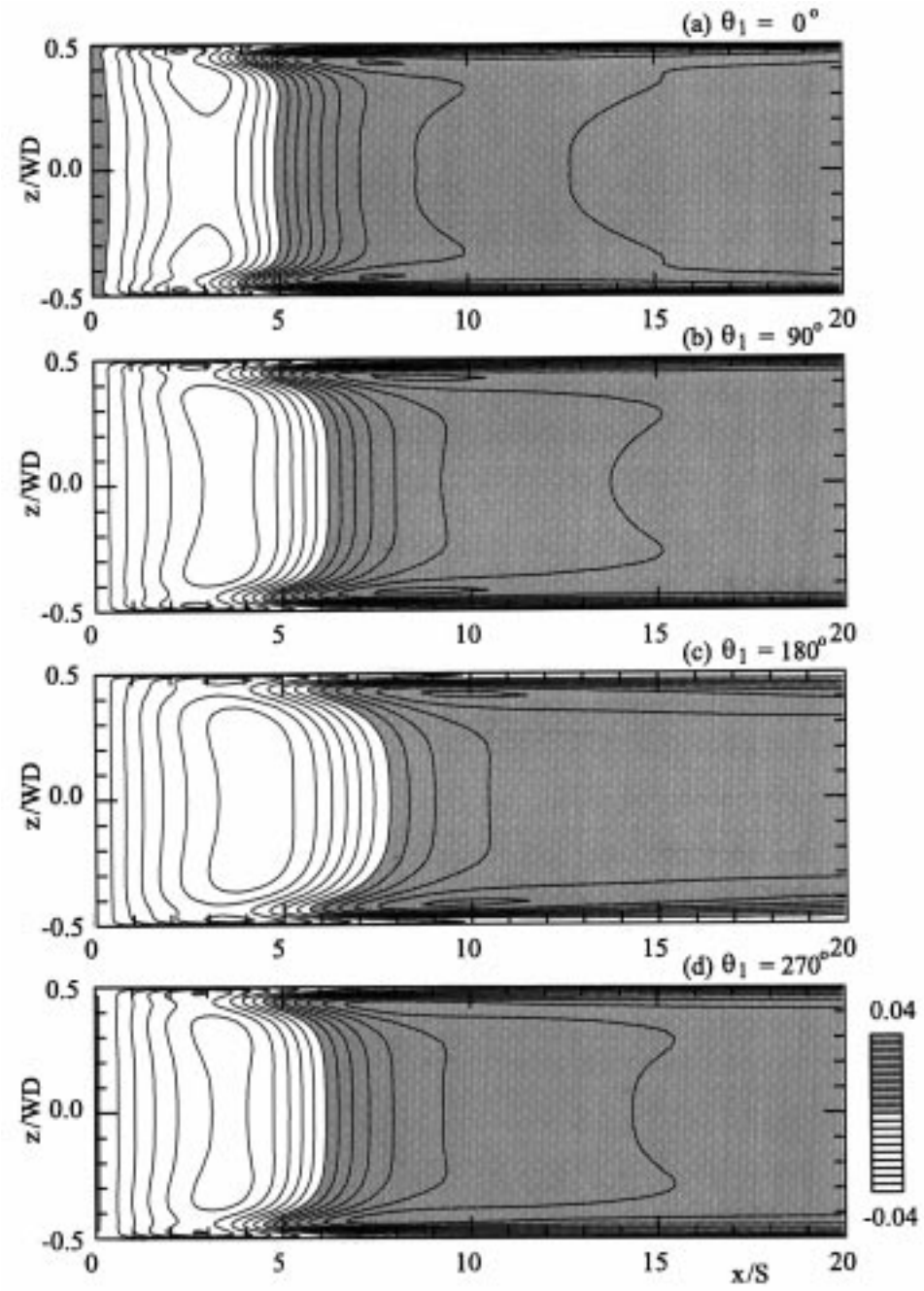

Fig. 8. C_f contours on the heated wall.

The contours of the Nusselt number Nu on the heated wall corresponding to those of C_f plotted in Fig. 8 are shown in Fig. 9. The gray tone level corresponds to the level of Nusselt number. The calculated thermal fields are symmetric with respect to the duct centerline. Again, the 2D region can be observed in the middle region of the heated wall. Maximum Nusselt

Table 1
Locations and values of Nu_{max}

θ_1 degree	0	45	90	135	180	225	270	315	360
x_{max}/S	4.52	4.52	4.94	6.00	6.21	6.00	4.94	4.52	4.52
$\lvert z_{max}/WD \rvert$	0.45	0.45	0.45	0.43	0.43	0.43	0.45	0.45	0.45
Nu_{max}	2.54	2.45	2.27	1.89	1.80	1.90	2.18	2.45	2.54

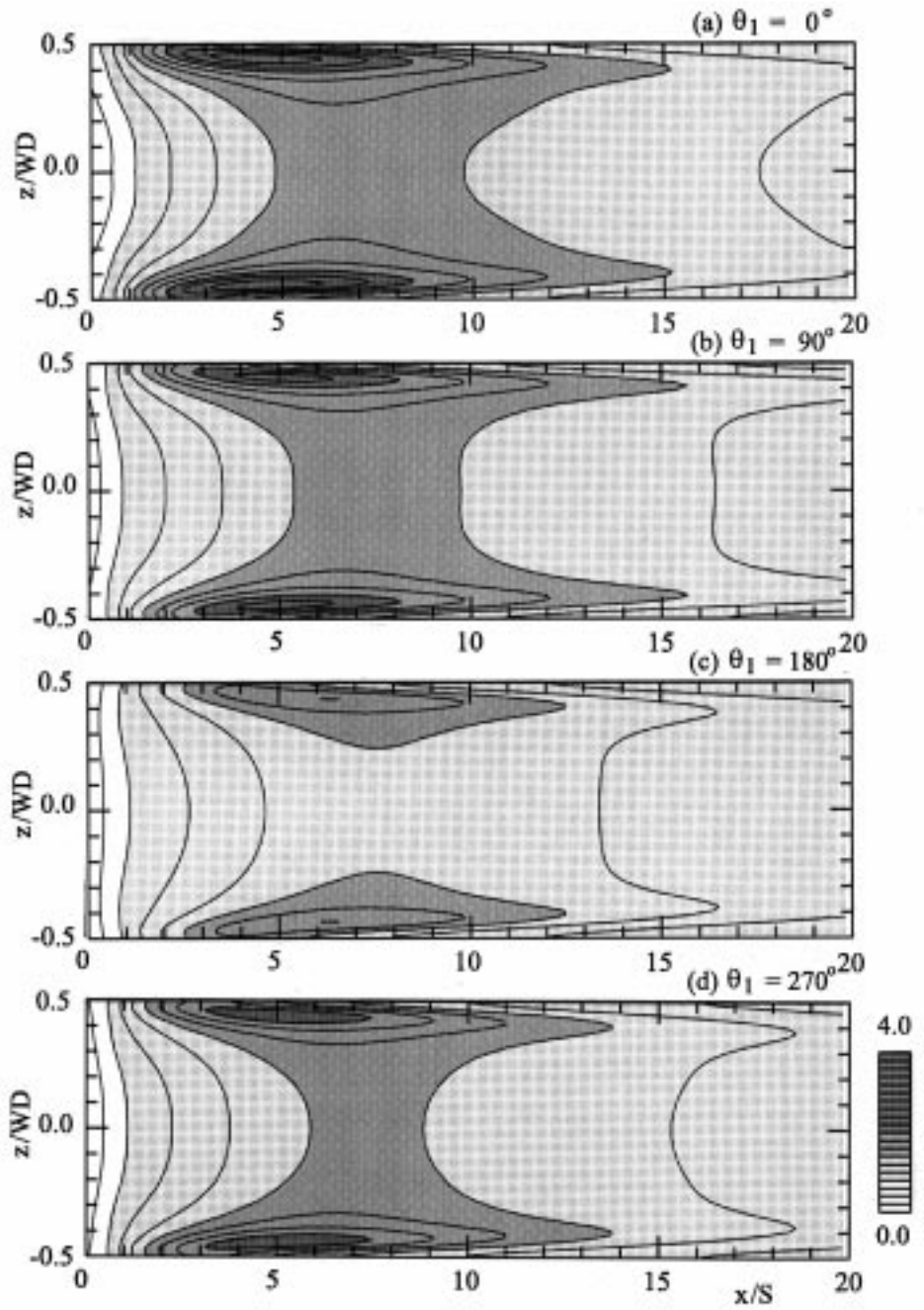

Fig. 9. *Nu* contours on the heated wall.

numbers, Nu_{max}, are located symmetrically near both side walls and not on the centerline of the heated wall similar to the cases of pure forced convection [1].

The value of Nu_{max} and its streamwise and spanwise locations are summarized in Table 1. Nu_{max} exhibits its highest value at $\theta_1 = 0^\circ$ $(=360^\circ)$ and lowest value at 180°. It appears at the most upstream position for the case $\theta_1 = 0^\circ$, while it is located at the most downstream position for the case $\theta_1 = 180^\circ$. The spanwise position of Nu_{max} appears slightly closer to the duct center at $\theta_1 = 180^\circ$ than 0°. However, it remains in any case close to the side walls.

The skin friction coefficient distribution along the centerline are compared among the studied four cases

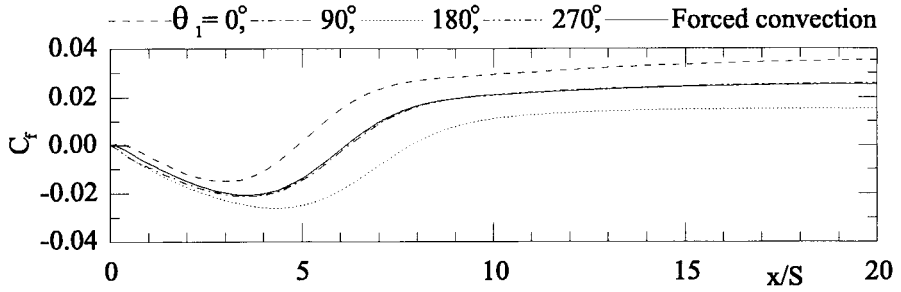

Fig. 10. C_f distributions along the centerline.

in Fig. 10. The result of a pure forced convection case (unheated case) is also shown in this figure as a reference. C_f values are particularly bigger over the entire range of the x-location when $\theta_1 = 0^\circ$, and smaller when $\theta_1 = 180^\circ$, compared to the pure forced convection case. The reason for this is that the main flow direction (x-direction) is exactly parallel to the buoyancy direction in these two cases. Hence, the buoyancy driven acceleration near the heated wall becomes maximum, when $\theta_1 = 0^\circ$ and minimum when $\theta_1 = 180^\circ$. Two horizontal cases ($\theta_1 = 90^\circ$, 270°) show little deviation from the pure forced convection case. This again suggests that the buoyancy level $Ri^* = 0.03$ is not large enough to alter the velocity field noticeably in the cases of horizontal flows. A careful observation indicates that even in such cases a slight deviation can be found near the step ($0 < x/S < 3$) where fluid velocity is quite small. The secondary recirculation region is observed only in the case of $\theta_1 = 270^\circ$ but not in the case of $\theta_1 = 270^\circ$ in Fig. 5.

Fig. 11 shows the fluid temperature contours in the duct center plane calculated for the two cases of $\theta_1 = 90^\circ$ and 270°. Thicker tone correspond to the higher temperature in this figure. The temperature difference between two neighboring contourlines in Fig. 11 corresponds to 0.8 K if the step height, S, is presumed to be 10 mm. There is no noticeable difference between the two distribution patterns downstream of the reattachment point ($x_r/S \simeq 6.2$). However inside the main recirculation region, especially near the origin of the coordinate system, slight difference is observed between these two cases. This difference may be related to the fact that the secondary recirculation region exists only in the case of $\theta_1 = 270^\circ$ but not in the case of $\theta_1 = 90^\circ$ as is seen in Fig. 5.

In experimental studies, flow direction is often set to be horizontal like such cases as $\theta_1 = 90^\circ$ and 270°, in order to minimize the effects of buoyancy on the flow field. Considering the above figures and discussions, keeping the flow direction horizontal seems to be effective for this purpose. Experimental results must be examined yet very carefully. For instances, if one

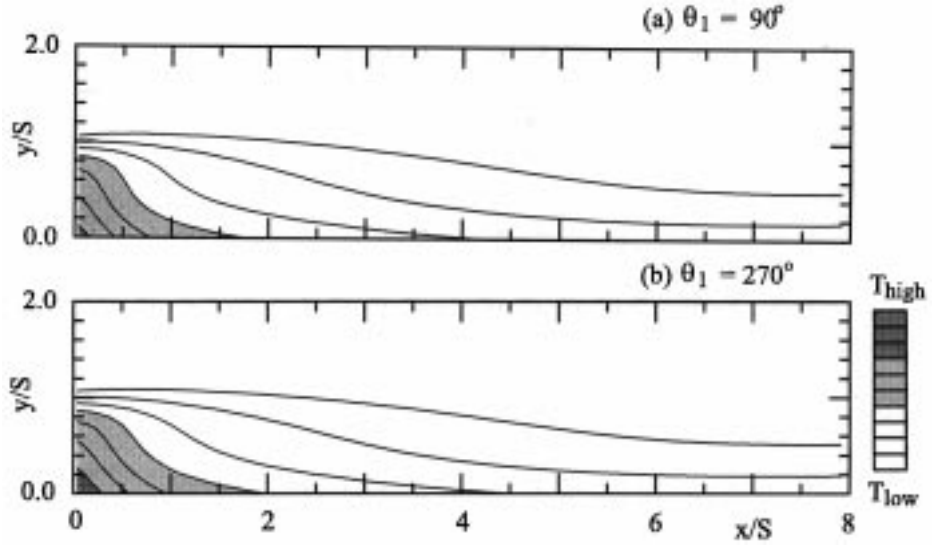

Fig. 11. Temperature contours in the central plane $z/W_d = 0$.

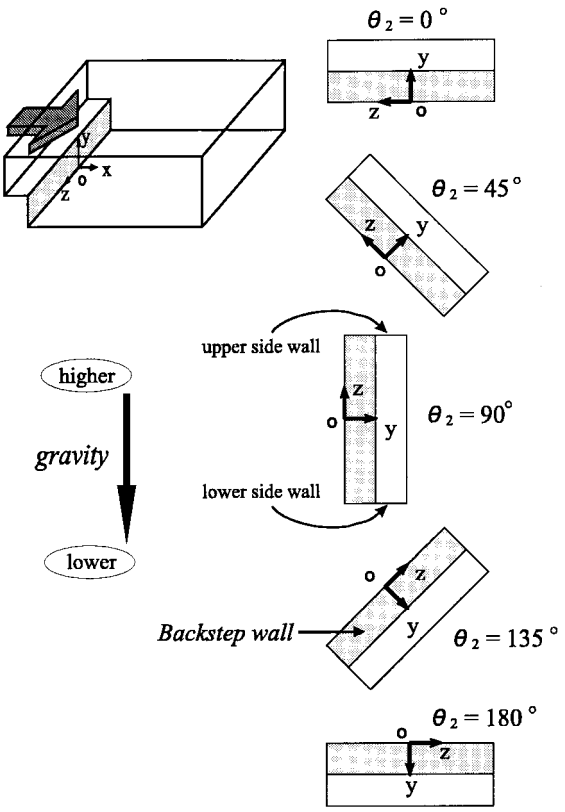

Fig. 12. Change of duct posture with θ_2.

focuses on the downstream of the reattachment point, buoyancy effects are actually small enough there for the cases of $\theta_1 = 90^\circ$ and 270° at $Ri^* = 0.03$. Therefore, flow can be judged to be a pure forced convective flow. On the other hand, in the main recirculation region, where the flow is very slow, flow and temperature fields can be affected even at this relatively low buoyancy level. Therefore, flow must be judged to be in the mixed convective flow regime.

3.3. Effects of the rolling angle θ_2

The effects of the rolling angle, θ_2, is studied here. θ_2 shown in Fig. 1 is changed from 0° to 180° while θ_1 is kept constant at 90°. This is schematically illustrated in Fig. 12. It should be noted that the side wall at $z/WD = 0.5$ is always on the higher level than the other side wall at $z/WD = -0.5$ in the range of $0^\circ < \theta_2 < 180^\circ$. The side wall at $z/WD = 0.5$ will then be called as the 'upper side wall' while the side wall at $z/WD = -0.5$ as the 'lower side wall' in this section. The cases of $\theta_2 = 0^\circ$, 180° at $\theta_1 = 90^\circ$ are equivalent to the cases of $\theta_1 = 90^\circ$, 270° at $\theta_2 = 0^\circ$. The flow and thermal fields in these two cases were found to be symmetric about the duct centerline. The results for other values of the rolling angle in the range $0^\circ < \theta_2 < 180^\circ$, on the other hand, show strong asymmetry. Therefore, the discussion will basically be focused on the cases in which the asymmetric flow and thermal fields are observed.

Table 2
Locations and values of Nu_{max}

θ_2 degree	0	15	30	45	90	135	180
x_{max}/S	4.94	4.73	4.52	4.30	4.09	4.30	4.94
z_{max}/WD	±0.45	−0.45	−0.45	−0.45	−0.45	−0.45	±0.45
Nu_{max}	2.27	2.67	2.98	3.20	3.41	3.05	2.18

The contours of the skin friction coefficient, C_f, on the heated wall are presented in Fig. 13 for four cases of different values of θ_2 namely $\theta_2 = 15^\circ$, 45°, 90°, 135°. The upper side wall is drawn on the upper side of the paper in each figure so that an upper location in the figure corresponds to a higher location. Asymmetry of the contours about the duct centerline is evident in these figures. The borderline between the shaded area and the white area around $x/S \simeq 5$ corresponds to the position of reattachment point. It can be seen in Fig. 13 that the main flow reattaches the heated wall at a more upstream location in lower half of the duct ($z/WD < 0$) than in the other half.

The contours of the Nusselt number, Nu, on the heated wall corresponding to those of C_f illustrated in Fig. 13 are shown in Fig. 14. The gray tone level corresponds to the level of Nusselt number. Maximum Nusselt number, Nu_{max}, are obtained at two positions lying symmetrically with respect to the centerline only when $\theta_2 = 0^\circ$, 180° as has been observed in Fig. 9(b) and (d). In all the other cases plotted in Fig. 14, Nu_{max} can be obtained only at one position, near the lower side wall ($z/WD = -0.5$). Although a clear peak of Nusselt number is still observed near upper side wall ($z/WD = 0.5$) in the case of $\theta_2 = 15^\circ$, no peak can be detected in other cases as is observed in Fig. 14.

The effects of θ_2 on the value of maximum Nusselt number, Nu_{max} and its streamwise and spanwise locations are summarized in Table 2. The maximum Nusselt number, appears at the most upstream position in the case $\theta_2 = 90^\circ$ and takes the highest value. θ_2, however, has little effect on the spanwise position of the maximum Nusselt number.

In the pure forced convection case [1], the maximum Nusselt number is obtained at two positions near the side walls symmetrically located with respect to the centerline. This was because of the downwash flow which symmetrically exist at such spanwise positions. The downwash flow brings relatively cooler fluid to near the heated bottom wall, causing the large temperature gradient and consequently high Nu there.

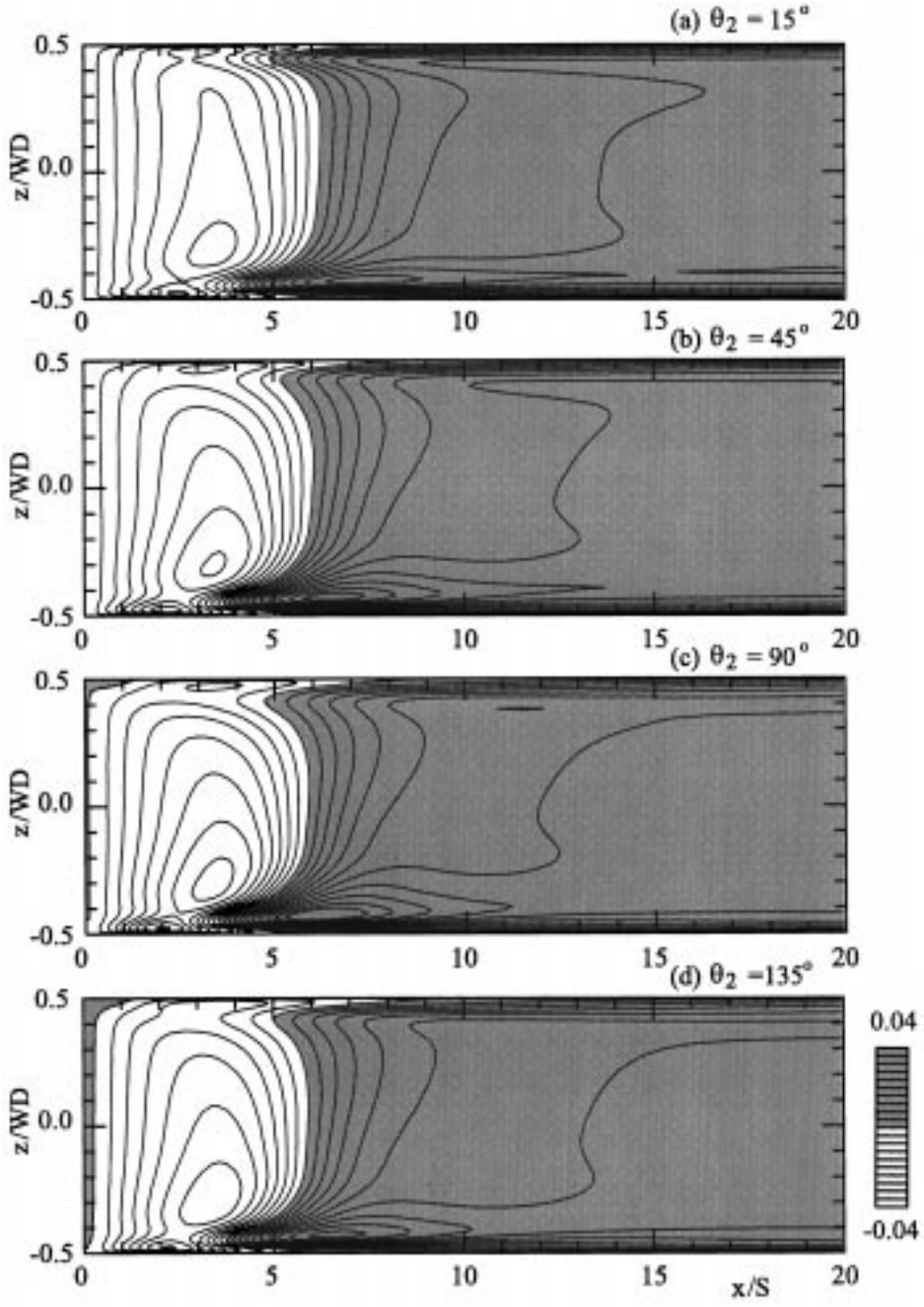

Fig. 13. C_f contours on the heated wall.

Therefore it would be natural to think that the effects of the rolling angle θ_2 on the downwash flow should be related to the spanwise asymmetry of the Nusselt number distribution observed in Fig. 14.

In order to discuss the three-dimensionality of the flow and thermal fields more in detail, velocity field in a y-z cross-section of the duct is examined at three different streamwise locations for the case of $\theta_2 = 90°$. Velocity vector of the cross-sectional secondary flow and contour of the streamwise velocity U in the three streamwise cross-sectional planes are shown in Fig. 15. The shaded areas here correspond to the region where U velocity is positive. Fig. 16, on the other hand, shows contours of the fluid temperature normalized

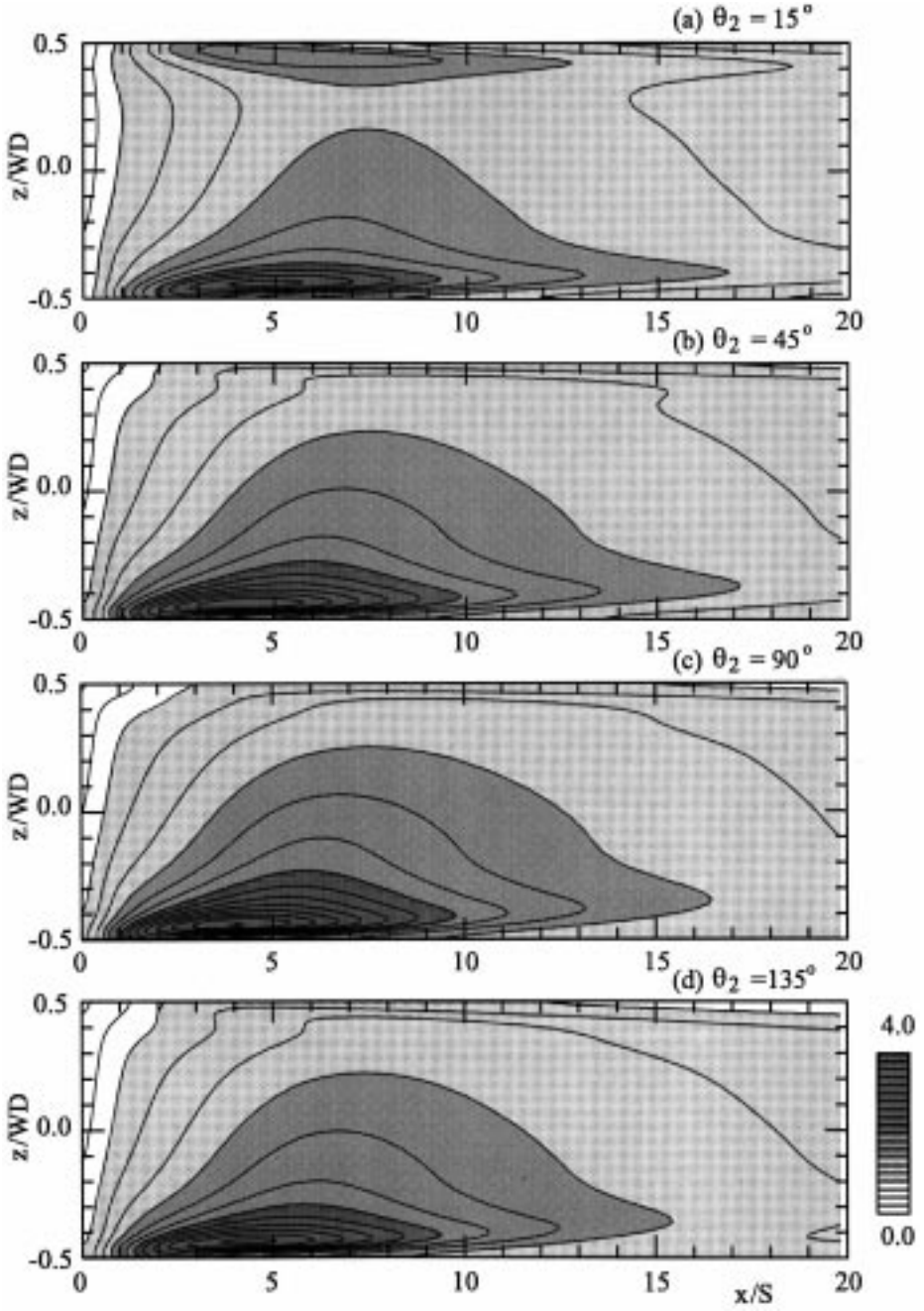

Fig. 14. *Nu* contours on the heated wall.

with $(T_{max} - T_{min})$, where T_{max} and T_{min} correspond to the maximum and minimum temperature in each cross section, respectively. The gray tone level correspond to the value of the fluid temperature. The upper side wall at $z/WD = 0.5$ is drawn on the left hand side of the paper in Figs. 15 and 16. The left hand side of these figures is higher than the right hand side.

At the location $x/S = 0.5$, as is observed in Fig. 16, temperature contour already shows asymmetry. In the region of $0 < y/S < 1$, where small velocity is expected to exist, the velocity vectors show that fluid flows upward. It is seen in Fig. 15 that U contour protrudes toward the heated wall at the position around $|z/WD| = 0.45$ at the location $x/S = 4.0$. This is

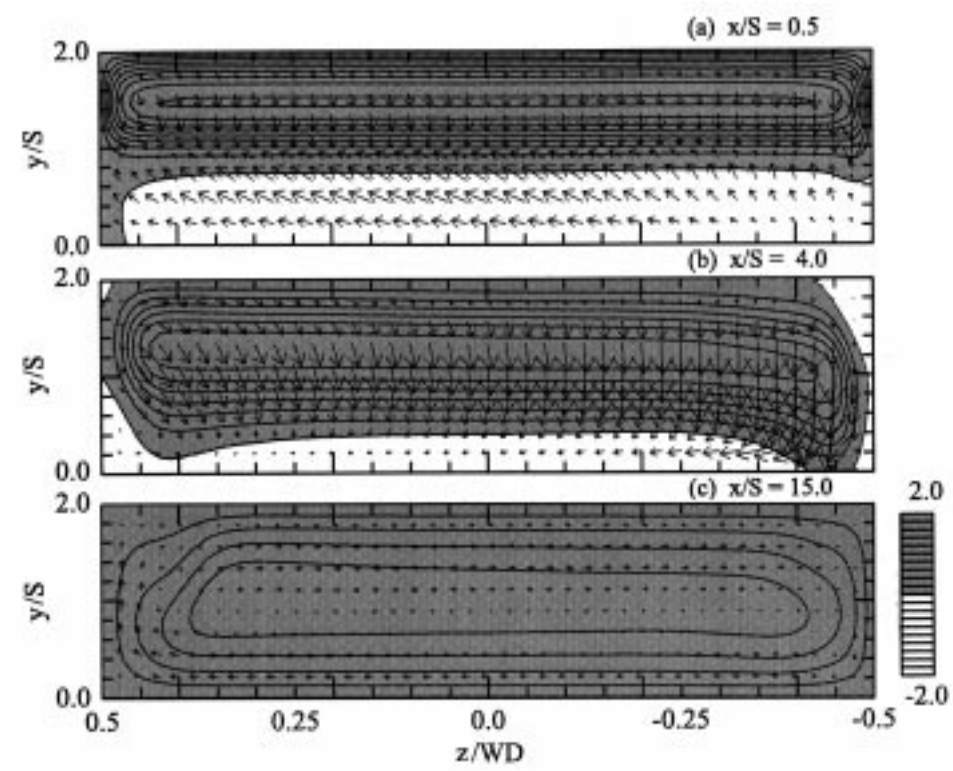

Fig. 15. U/U_{in} contours and V–W vector plots.

caused by the downwash flow directed toward the heated wall observed at such spanwise positions. However, comparison of the velocity vectors at such spanwise positions shows that the downwash flow at $z/WD = -0.45$ is obviously more prominent than that at $z/WD = 0.45$. The temperature contours show that relatively cooler fluid approaches the heated wall at positions around $z/WD = -0.45$. This is effective to keep the wall temperature lower, therefore, to result in higher Nusselt number there. However, this low temperature region is not observed at the position around $z/WD = 0.45$. At the location $x/S = 15.0$, no prominent secondary flow in y-z plane is observed. Yet a careful observation suggests that there exists a large scale flow rotation. Fluid near the heated wall is directed upward (to the left side in the figures) while it is directed downward (to the right side in the figures) near the opposite unheated wall.

4. Conclusions

Three-dimensional numerical simulations have been carried out for mixed convective flows over a backward-facing step in a duct. The effects of two inclination angles, the pitch angle and the rolling angle on the flows mentioned above were studied under the condition of $Re = 125$ and $Ri^* = 0.03$. The following conclusions were obtained.

1. Both of pitch angle and rolling angle significantly affect the flow and thermal fields. The positions of x_r, x_p and x_s on the centerline of the heated wall shift with θ_1.
2. When θ_1 is changed keeping θ_2 to be zero degree, positions of the maximum Nusselt numbers are symmetrically obtained at the positions on the heated wall near the two side walls, similar to the cases of pure forced convection. The value of maximum Nusselt number and its position are affected by the value of θ_1. The maximum Nusselt number appears at the most upstream position in the case of $\theta_1 = 0^\circ$ and takes the highest value. Buoyancy effects seem to be relatively small in the cases of horizontal flows, especially for the flow and thermal fields downstream the reattachment point.
3. When θ_2 is changed keeping θ_1 to be 90°, the flow and thermal fields become asymmetric about the duct centerline. The downwash flow directed toward the heated wall is prominent only near the lower side wall, resulting only one prominent peak of Nusselt number, Nu_{max}, there. The maximum Nusselt number appears at the most upstream pos-

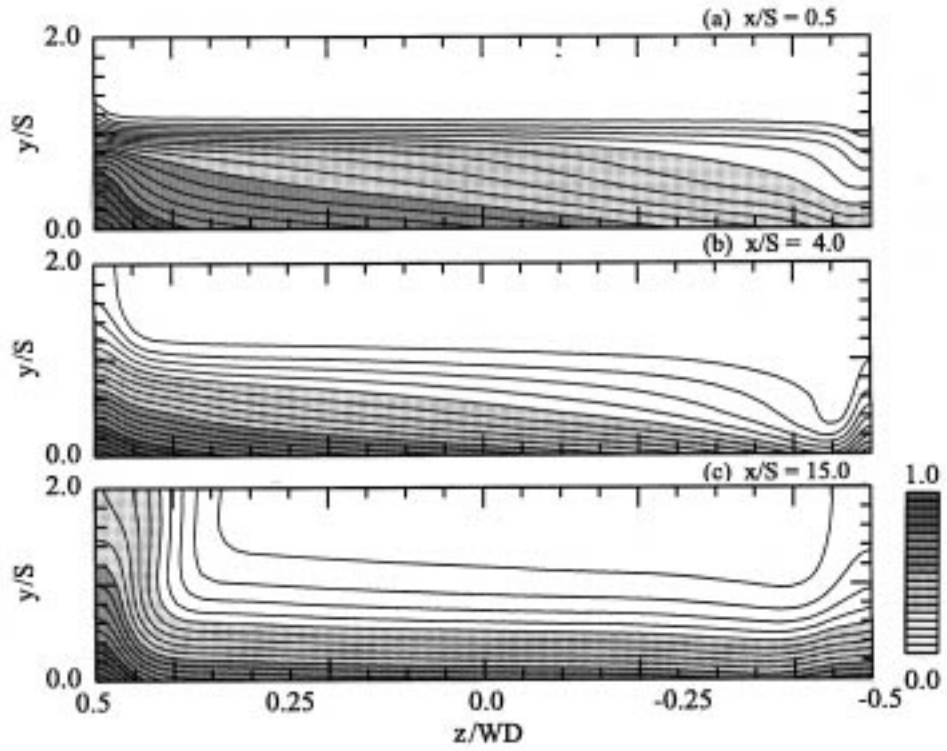

Fig. 16. Normalized temperature $(T - T_{min})/(T_{max} - T_{min})$ contours.

ition in the case $\theta_2 = 90^\circ$ and takes the highest value. However θ_2 has little effect on the spanwise position of the maximum Nusselt number.

References

[1] H. Iwai, K. Nakabe, K. Suzuki, A three-dimensional numerical study on heat transfer characteristics of backward facing step flow in a rectangular duct, in: B. Wang (Ed.), Heat Transfer Science and Technology 1996, Higher Education Press, Beijing, 1996, pp. 541–546.

[2] P.M. Worsoe-Schmidt, G. Leppert, Heat transfer and friction for laminar flow of gas in a circular tube at high heating rate, Int. J. Heat Mass Transfer 8 (1965) 1281–1301.

[3] S.V. Patankar, S. Ramadhyani, E.M. Sparrow, Effect of circumferentially nonuniform heating on laminar combined convection in a horizontal tube, Trans. ASME: J. Heat Trans 100 (1978) 63–70.

[4] N. Ramachandran, B.F. Armaly, T.S. Chen, Measurements and predictions of laminar mixed convection flow adjacent to a vertical surface, Trans. ASME: J.Heat Trans 107 (1985) 636–641.

[5] B.J. Baek, B.F. Armaly, T.S. Chen, Measurements in buoyancy-assisting separated flow behind a vertical backward-facing step, Trans. ASME: J.Heat Trans 115 (1993) 403–408.

[6] H.I. Abu-Mulaweh, B.F. Armaly, T.S. Chen, Measurements of laminar mixed convection in boundary-layer flow over horizontal and inclined backward-facing steps, Int. J. Heat Mass Trans 36/37 (1993) 1883–1895.

[7] H.I. Abu-Mulaweh, B.F. Armaly, T.S. Chen, Measurements in buoyancy-opposing laminar flow over a vertical backward-facing step, Trans. ASME: J. Heat Trans 116 (1994) 247–249.

[8] J.T. Lin, B.F. Armaly, T.S. Chen, Mixed convection in buoyancy-assisting, vertical backward-facing step flows, Int. J. Heat Mass Trans 33 (10) (1990) 2121–2132.

[9] J.T. Lin, B.F. Armaly, T.S. Chen, Mixed convection heat transfer in inclined backward-facing step flows, Int. J. Heat Mass Trans 34 (6) (1991) 1568–1571.

[10] B. Hong, B.F. Armaly, T.S. Chen, Laminar mixed convection in a duct with a backward-facing step: the effects of inclination angle and Prandtl number, Int. J. Heat Mass Trans 36 (12) (1993) 3059–3067.

[11] S.V. Patankar, D.B. Spalding, A calculation procedure for heat, mass and momentum transfer in three-dimensional parabolic flows, Int. J. Heat Mass Transfer 15 (10) (1972) 1787–1806.

[12] R.K. Shah, A.L. London, Laminar Forced Convection in Ducts, Academic Press, New York, 1978.